rijksuniversiteit
groningen

LOMONOSOV MOSCOW
STATE UNIVERSITY

INTERNSHIP REPORT

Organic Field-Effect Transistors fabrication and characterization

Author:
Koen BLAAUW (s2511908)

Supervisors:
Prof. Dr. M. S. PCHENITSCHNIKOV
Prof. Dr. D. Yu. PARASCHUK

Daily supervisor:
Dr. V. A. TRUKHANOV

Abstract

This report discusses my findings during my internship in the Organic Electronics group lead by Dmitry Yu. Paraschuk at Lomonosov Moscow State University. The group focusses on the development of organic electronics including organic solar cells, plastic photovoltaics, organic field-effect devices and Raman spectroscopy. During this internship, I worked in collaboration with postdoctoral researcher Vasya Trukhanov who is currently studying organic field-effect devices and aims to design both high charge mobility, organic field-effect transistors (OFET) as well as efficient organic light-emitting transistors (OLET). These projects involve finding the most promising molecules for the active layer, as well as developing efficient methods of electron and hole injection into the active layer. Samples based on various derivatives of thiophene-phenylene co-oligomers were fabricated and both electrophysical and electroluminescent properties were analysed.

August 22, 2019

1 Introduction

Organic semiconductors (OSCs) have a unique combination of mechanical, electrical and optical properties which make them essential components in the development of a new generation of low-cost, flexible and transparent electronics.[1] The past 30 years, researchers spend significant efforts on the development of electronic devices based on OSCs with the nowadays commercially available organic light-emitting diode (OLED) display as a well-known example of their accomplishments.[2] Pixels in an OLED display are currently still being driven by inorganic thin-film transistor (TFT) backplanes based on polycrystalline silicon. As this obstructs the potential of fully organic electronics, there is need for organic field-effect transistors (OFET).[3] The newest concept in the field is the organic light-emitting transistor (OLET)[4] which integrates light emission from OLED and electrical switching from OFET.[5] Apart from display fabrication with simpler driving circuits, the most advanced OLETs possess the potential of being bright nanoscale light sources enabling the realization of the electrically pumped organic laser.[6]

Present day research focusses on identification of high charge-mobility OSCs as device efficiency and speed generally improves with increasing mobility.[7] Significant improvements in mobilities have been reported in recent years. However, a number of the values found were shown to be the result of erroneous evaluation of non-ideal OFET characteristics resulting in large mobility overestimations.[1] A critical review of published data revealed that reliable hole and electron mobility values of 20 and 10 $cm^2V^{-1}s^{-1}$, respectively, have yet to be achieved.

Materials potentially used in OLET, are apart from a high mobility, prone to the additional requirement of having bright luminescence. Finding materials possessing this specific combination is challenging as the former is usually achieved in isolated molecules while the latter requires tight molecular packing.[8] One way to overcome this problem is by external doping of the host with a highly luminescent molecule collecting excitation energy from the host. Recently, a novel and more advantageous concept of self doping was introduced and proved on thiophene-phenylene cooligomers (TPCO).[8] During this internship, the charge transport and luminescence capabilities of TPCO were explored further.

1.1 Theory

This section aims to describe OFET (and OLET) operation. First the classical silicon MOSFET operation will be addressed by means of a derivation of the standard Shockley equations. Next the main difference between MOSFET and OFET will be highlighted.

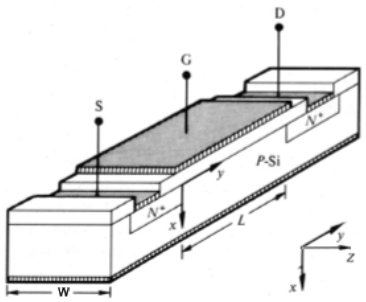

Figure 2: Schematic of a typical n-channel MOSFET with channel length L and channel width W.

Consider the device shown in figure 2. A typical n-channel MOSFET consists of two n^+ channel contacts within a p-type substrate combined with a dielectric layer and gate electrode. By biasing the gate V_g to the proper sign (+ for an n-type channel) an inversion layer is induced

at the insulator-semiconductor interface which creates an conductive channel between the source and drain contacts. Applying a drain voltage V_d results in a non-constant potential across the channel V_y causing charges to flow from source to drain. According to Ohm's law this current I_d is equal to

$$I_d = -\int_S \vec{J} \cdot d\vec{a} = -\int_S q\mu n \vec{E} \cdot d\vec{a} = -\int_S q\mu n(x,y) \frac{dV_y}{dy} \cdot dxdz = -W\bar{\mu}Q_N \frac{dV_y}{dy}, \tag{1}$$

where $\bar{\mu}$ is the effective mobility and Q_N is the inversion layer charge density per unit area. The expression can be simplified by integrating both sides along the channel length:

$$\int_{y=0}^{y=L} I_d \dot{dy} = I_d L = -W\bar{\mu} \int_{V_y=0}^{V_y=V_d} Q_N dV_y. \tag{2}$$

According to the gradual channel approximation, the charge density in the channel, Q_N, follows directly form the product of the capacitance, C_i, and the effective voltage drop across the insulator, $V_{eff} = V_g - V_t - V_y$, where V_t is the threshold voltage, accounting for trapped and static charges. Substitution for $C_i \cdot V_{eff}$ and integration over the channel potential result in the following expression:

$$I_d = \frac{W\bar{\mu}}{L} \int_{V_y=0}^{V_y=V_d} (C_i \cdot V_{eff}) dV_y = \frac{C_i W\bar{\mu}}{L} \int_{V_y=0}^{V_y=V_d} (V_g - V_t - V_y) dV_y = \frac{WC_i\bar{\mu}}{L} \Big[(V_g - V_t)V_d - \frac{V_d^2}{2} \Big]. \tag{3}$$

Implementing the approximations valid in the linear ($V_g \gg V_d$) and saturation ($V_d = V_g - V_t$)[1] regimes result in the classical Shockley MOSFET equations:

$$\text{Linear regime:} \quad (V_g \gg V_d) \qquad I_d = \frac{WC}{L}\mu(V_g - V_t)V_d, \tag{4}$$

$$\text{Saturation regime:} \quad (V_d = V_g - V_t) \qquad I_d = \frac{WC}{2L}\mu(V_g - V_t)^2. \tag{5}$$

In contrast to MOSFET, which operates based on charge *inversion*, OFET is ideally based on charge *accumulation*[9].[10] A schematic of basic OFET operation based on p-type conductivity is shown in figure 5. In the OFF-state, hole injection is prevented by an energy barrier which height is, amongst other factors, dependent on the metal work function and the ionization energy of the semiconductor. In the ON-state, a negative bias V_g is dropped over the insulator and over the semiconductor near the interface, giving rise to band bending as shown in the figure on the right. Although the height of the barrier is fixed due to energy pinning at the interface, the width reduces significantly as a function of V_g (and V_d). This allows carriers to cross the barrier by means of thermally excitation or tunnelling enabling carrier transport between source and drain.

[1] Saturation occurs when $V_d \geq V_g$ such that at some point in the channel $V_{eff} = 0$. From this point on, the channel is pinched off i.e. no inversion layer forms. When pinchoff occurs, the inversion length is smaller than the channel length. As literature shows that the resistance of the depleted part of the channel can be disregarded,[9] channel shortening due to saturation is incorporated in the transport equation by replacing V_d with $V_g - V_t$.

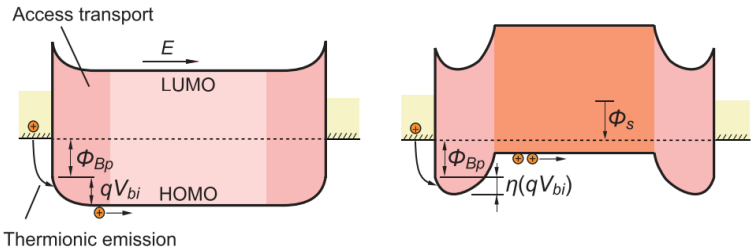

Figure 3: Energy diagrams of OLET illustration the operating principle. Upon applying a gate bias V_g, the device switches from the ON (Left) to the OFF (right) state. Φ_{Bp} and $qVbi$ are the "Schottky barrier" and build-in-potential respectively. Note that $\Phi_{Bp} = E_{HOMO} - \Phi_m$, where E_{HOMO} is the energy level corresponding to the HOMO and Φ_m is the metal work function. Figure adapted from Xu *et al.*[11]

Charge mobilities observed in organic materials are often orders of magnitude smaller compared to the mobilities observed in their inorganic counterparts ($\mu = 10$ cm^{2}V^{-1}s^{-1} compared to 500 cm^{2}V^{-1}s^{-1} respectively). This difference is predominantly caused by a different transport mechanism. In organic semiconductors, electron and hole transport occurs through unoccupied density of states (DOS) corresponding to the lowest unoccupied molecular orbital (LUMO) and occupied DOS corresponding the highest occupied molecular orbital (HOMO) respectively. As a result of disorder and a variation in interaction energies in organic materials, charge transport occurs more complicated than free carriers moving in delocalized bands (as happening in inorganic crystals).[12] Instead spatially and energetically separated transport sites are present in which charges move by means of a thermally activated tunnelling mechanism, denoted as hopping.[13]

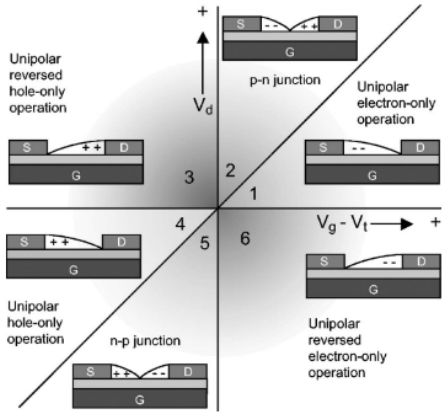

Figure 4: Sketch showing all operating regimes for a typical ambipolar transistor as a function of gate and drain bias. Figure from Smits *et al.*[12]

A third feature that distinguishes organic from inorganic transistors, is the capability of single layer ambipolar transport. As channel formation in OLET is based on charge accumulation instead of inversion, it is possible to accumulate charges of different sign, at different positions within the channel. As mentioned earlier, charge accumulation occurs as a result of the drop in the effective potential, $V_{eff} = V_g - V_t - V_y$, across the insulator interface. Notice that when $V_d = V_g - V_t$, the effective potential at the drain contact equals zero. Hence there is no accumulation of charges and the channel is pinched off. Upon further increase of the drain potential, the pinchoff location, x_0, moves into the channel towards the source contact. Realize that the effective potential changes sign at x_o resulting in the accumulation of the opposite carrier.

Applying the correct combination of gate and drain biases thus results in simultaneous accumulation of both electrons and holes (see figure 4). Caused by the drain potential V_d, electrons and holes transport through LUMO and HOMO respectively, until the meet each other. At this position a narrow transition region, acting as a pn-junction will develop. Within this region, electrons and holes will recombine resulting in the emission of light.[12]

1.2 Research Aim

The creation of energy efficient OLET, i.e., high conversion coefficient of electrical energy into light, is one of the most important unresolved problems in the field of organic optoelectronics. Most important with respect to device performance, is the choice of molecules, used for the active layer. The molecules should have high luminescence quantum yield, should crystallize in lamellar crystals and need to have balanced electron and hole mobilities.[14]

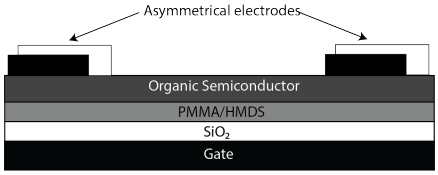

Figure 5: Schematic cross section showing the device geometry of organic field-effect (without asymmetrical electrodes) and organic light emitting transistors used for all experiments described in this report.

Apart from the active layer, device performance is partially determined by the efficiency of charge injection at the electrode-semiconductor interface. An offset between the metal work function of the electrode and the HOMO and LUMO levels of the organic result in energy barriers for charges moving from the electrode into the channel as depicted in figure 5.[11] The energy barriers and corresponding contact resistance can be reduced by minimizing, the energy offset, which explains the use of asymmetrical source and drain electrodes (see figure 5). Highly efficient OLETs therefore require a highly luminescent organic semiconductor in combination with energy-matching source and drain electrodes. The group of Organic Electronics is currently working on this novel task. The goals of this project are summarized as follows:

1. Find the most promising molecules for the active layer of OLET.
2. Develop the most promising method for the formation of the active layer.
3. Suggest methods for efficient injection of holes and electrons into the active layer.
4. Identify the relationship between molecular structure, impurities, crystalline packaging and photoelectrical properties.

Besides the former, I contributed to a project focussed on the creation of high charge mobility $n-$channel field effect transistors. As mentioned earlier, organic semiconductors that combine ease of synthesis, stability and high carrier mobility ($\mu > 1$ cm^{2}V^{-1}s^{-1}) are not yet know. Moreover, organic semiconductors with high electron mobility are developed significantly less than high hole mobility semiconductors. The goals of this project correspond to the previously mentioned goals with the exception of the search for efficient hole injection.

2 Approach

The choice of molecules used for the active layer in OLET, is decisive with respect to device performance. According to recent studies,[15] the previously stated requirements, e.g. high luminescence quantum yield, lamellar crystallization and balanced electron and hole mobilities are well met by thiophene-phenylene co-oligomers which will therefore be used as active layer for this project. The general approach is the following:

1. Identification of most promising thiophene-phenylene oligomers using quantum chemical calculations
2. Chemical synthesis of new thiophene-phenylene oligomers based on quantum chemical calculations and experimental data
3. Creation of unipolar and ambipolar transistors using various fabrication techniques.
4. Measure and study the transistors electrical and electroluminescent characteristics.

During my internship, I was involved in steps 3 and 4, being the fabrication and analysis of transistors, made from various promising active layer - electrode combinations. More specifically, I was taught by postdoctoral researcher Vasya Trukhanov to fabricate organic transistors using the thermal vacuum evaporation technique and to perform the electrical characterization by means of measuring output and transfer characteristics.

Substrates

All experiments were performed using Si/SiO_2 substrates with an oxide layer thickness of 200 nm. The substrates were cleaned using toluene, acetone and isopropanol respectively, after which they were sonicated at 70°C for 20 min. Next, the substrates were cleaned using isopropanol and distilled water and treated for 15 minutes in a photo surface processor. Finally, a dielectric layer was added which has previously been reported to improve the structural quality of the grown organic crystals.[16,17] Half of the substrates were passivated by hexamethyldisilazane (HMDS) whereas the other half were treated with poly(methyl methacrylate) (PMMA). These layers were deposited by evaporation and spin coating respectively. The PMMA treated substrates were annealed at 70 °C overnight, which was increased to 110 °C two hours prior to the evaporation of the active layer.

Thermal Vacuum Evaporation

Thermal vacuum evaporation comprises the emission at a heated source of material which condenses on the substrate[18] within a vacuum chamber. The source is a wire or crucible electrically heated and containing the material to be evaporated. The evaporation rate is controlled by the amount of current being passed through the source and monitored using a quartz crystal microbalance (QCM). Provided that the density and acoustic impedance of the evaporated material are known, the layer thickness and evaporation rate can be calculated from the change in resonance frequency of the crystal.

For our experiments a molybdenum crucible and tungsten wires were used as a heat source. After evaporation of the active layer, shadow masks were used to pattern source and drain electrodes. In case of ambipolar transistors, asymmetric electrodes were realised using the shadow effect demonstrated in figure 6. The mask used corresponded to source and drain electrodes with a width of 100 μm and a channel length varying from 10 to 30 μm. This high

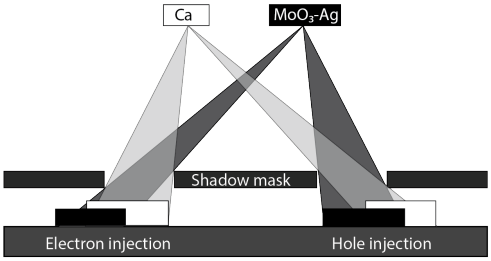

Figure 6: Shadow effect resulting in asymmetrical source-drain geometry for efficient hole and electron injection.

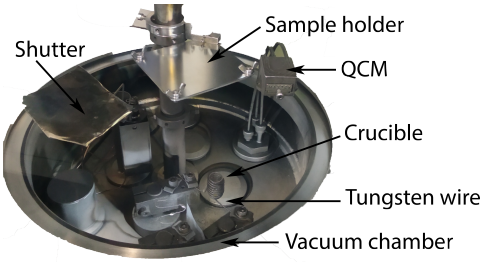

Figure 7: Picture of setup for thermal vacuum evaporation

W/L ratio was used to minimize fringing current and hence avoid mobility overestimation. A total of 20 devices was made per evaporation.

Electrical characterization

Electrical measurements were performed in an argon atmosphere using a Keithley 2636A source meter in combination with a Printeltech 100 Probestation and the corresponding software. Output and transfer characteristics were measured for varying biasing conditions from which field effect mobility μ and threshold voltages V_t were extracted according to the Shockley equations (eq. 4 and 5). At least five out of the twenty different devices, with channel lengths of 10, 15, 20, 25 and 30 μm were measured for each experiment. For each device, six transfer curves were extracted (three different drain voltages per two different gate voltage ranges.) with hysteresis. Furthermore the output characteristics were measured for three different gate voltages. Eventually the carrier mobility and threshold voltage was determined for both the forward and backward direction in the transfer curves.

Luminescence Analysis Program

Apart from the transistor fabrication and electrical characterization, I worked on a program used for the analysis of OLET luminescence. As mentioned earlier, the position of electron-hole recombination and hence the position of light emission varies under influence of the biasing conditions. The program was intended to analyse videos made of OLET light emission, perpendicular to the plane of the transistor, during gate voltage sweeps with constant V_d. More specifically, the program should extract the relative light intensity and light position, as a function of V_g. It was chosen to define the light position as the average distance between the light and the left electrode along the channel. A schematic of video frames, ass well as an illustration of the functionality of the program is shown in figure 14 in the appendix.

3 Results

During this internship, I have been involved in multiple experiments. Keeping the length and goal of this report in mind, only the results concerning my individual work on $CsCO_3$ electrodes and Oligophenylenes will here be discussed. An overview of the results of remaining experiments is given in the appendix. All mobilities and threshold voltages are given in units of $cm^2V^{-1}s^{-1}$ and volts respectively.

$CsCO_3$ vs. Ca Electrodes

As mentioned in section 1.2, OLET efficiency can be affected by contact resistance resulting from misalignment between the electrode work function and the energy levels of the transport bands. Recent studies report highly efficient electron injection based on novel low-work-function electrodes formed by thermally deposited $CsCO_3$[19].[20] Especially in combination with Al, highly conductive electrodes possessing a work function as low as 2.1 eV were reported to be obtained. During our project, we intended to determine the electron injection efficiency of $CsCO_3$−Al electrodes by direct comparison with normally used Ca (Φ_m = 2.9eV) electrodes. In total four experiments with different dielectric layers (HMDS and PMMA) and $CsCO_3$ layer thicknesses (413 = 3 nm, 419 = 4 nm) were conducted. All experiments were done using a well studied CF_3-PTTP-CF_3 (MAF) active layer.

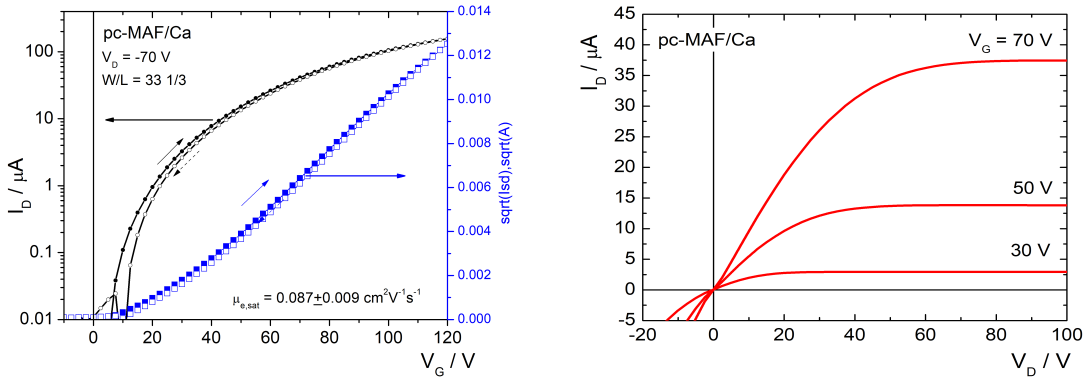

Figure 8: Transfer (Electrical characterization of MAF active layer combined with Ca electrodes (experiment 413) with left: transfer and right: output characteristics

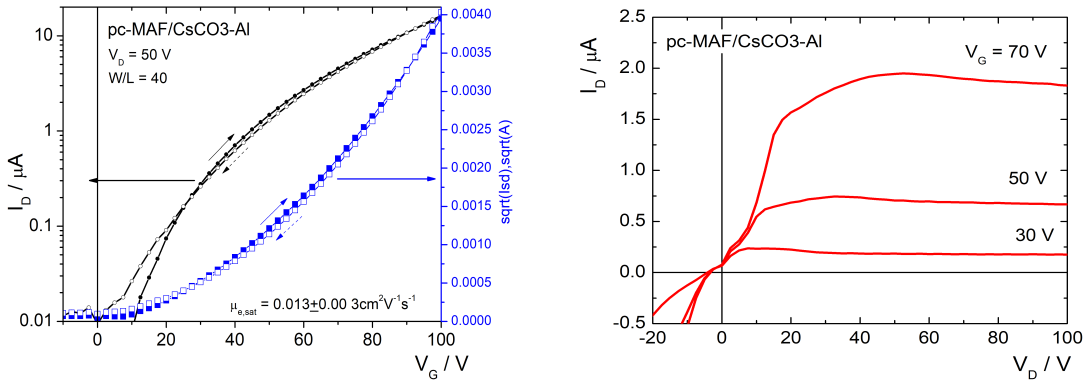

Figure 9: Electrical characterization of MAF active layer combined with $CsCO_3$-Al electrodes (experiment 412) with left: transfer and right: output characteristics

Figures 8 and 9 show the transfer and output curves of the best performing devices using Ca and $CsCO_3$−Al electrodes respectively. The Ca output characteristics at low drain voltages show ohmic-like behaviour, indicating low to negligible contact resistance. This in contrast to the $CsCO_3$ output characteristics where significant deviations from ideal can be observed. Furthermore the source-drain currents observed at various gate voltages, are approximately 20 times for Ca electrodes. The maximum hole mobility of 0.087 $cm^2V^{-1}s^{-1}$ for Ca electrodes, was found to be a factor 7 higher than the 0.013 $cm^2V^{-1}s^{-1}$ observed for $CsCO_3$ electrodes.

Date	Exp.	Act. Layer	Electrodes	Substrate	$\mu_{h,max}$	$\mu_{h,av}$	V_h	$\mu_{e,max}$	$\mu_{e,av}$	V_e
04.07	412	MAF	Ca	SiO_2/PMMA	-	-	-	0.087	0.0453±0.0011	17±9
04.07	413	MAF	$CsCO_3$−Al	SiO_2/PMMA	-	-	-	0.013	0.0047±0.0003	23±7
10.07	418	MAF	Ca	SiO_2/HMDS	-	-	-	0.122	0.0703±0.0022	37±11
10.07	419	MAF	$CsCO_3$−Al	SiO_2/HMDS	-	-	-	0.011	0.0019±0.0002	41±21

Table 1: $CsCO_3$ vs. Ca

The full statistics on these experiments are collected in table 1. Independent on the dielectric layer used, the average electron mobilities observed for Ca electrodes are at least a factor 10 higher than for $CsCO_3$ electrodes. Ca electrodes are furthermore found to result in lower threshold voltages, but the difference is small and is within the error margin.

Oligophenylenes Active Layers

This experiment was meant to study the dependence of OFET performance on oligomer length. Devices with active layers consisting of Oligophenylenes with four, five and six phenylene rings (denoted as 4P, 5P and 6P respectively) were fabricated and their electrical properties were characterized. All experiments were performed using PMMA as well as HMDS as dielectric layer. The transfer and output characteristics of the best performing device based on 4P, is shown in figure 10.

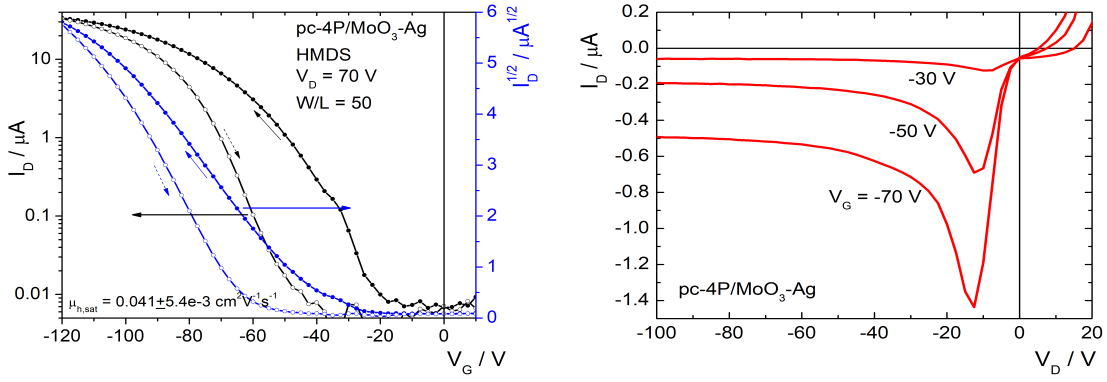

Figure 10: Electrical characterization of 4P Oligophenylene (experiment 437) with left: transfer and right: output characteristics.

The maximum hole mobility for 4P was found to be 0.041 $cm^2V^{-1}s^{-1}$ on HMDS. The transfer plot clearly shows significant hysteresis which is often attributed to trapped charges.[20] Furthermore, a rather large threshold voltage of approximately 30 V is observed. The output curves clearly show a decrease in I_d upon long exposure to the gate bias V_g. This feature is the result of degradation, as no gate leakage was observed at high V_d. The exact mechanism by which

degradation occurs, could not be determined. Finally a non-zero current is observed at $V_d = 0$. These features were found to be present in the 5P and 6P devices as well, as shown in figures 15 and 16 in the appendix.

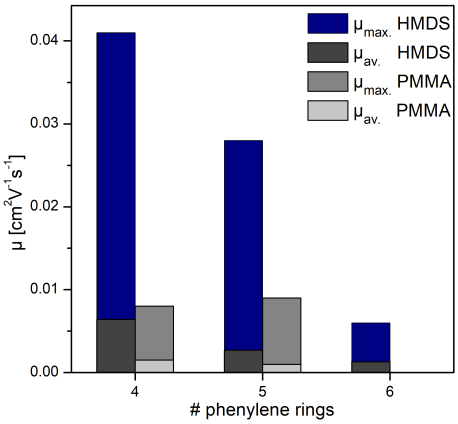

Figure 11: Histogram showing the maximum and average mobilities vs. the number of phenylene rings.

The full statistics on Oligophenylene experiments are shown in table 2. The maximum mobilities as well as the average mobilities are found to decrease for an increasing number of phenylene rings. On HMDS a prominent decrease in average mobility by a factor of approximately two is observed for each extra ring (see figure 11). In general, the mobilities on PMMA were found to be significantly smaller, than the mobilities found on HMDS. Finally no source-drain current at all was measured for 6P on PMMA. These results are in qualitative agreement with earlier experiments on the same compounds as shown in table 4 in the appendix.

Date	Exp.	Act. Layer	Electrodes	Substrate	$\mu_{h,max}$	$\mu_{h,av}$	V_h	$\mu_{e,max}$	$\mu_{e,av}$	V_e
25.07	436	pc-4P	MoO_3-Ag	SiO_2/PMMA	0.008	0.0015±0.0002	-15±23	-	-	-
25.07	437	pc-4P	MoO_3-Ag	SiO_2/HMDS	0.041	0.0064±0.0007	-28.7±16	-	-	-
24.07	438	pc-5P	MoO_3-Ag	SiO_2/PMMA	0.009	0.0010±0.0001	-34.5±19	-	-	-
24.07	439	pc-5P	MoO_3-Ag	SiO_2/HMDS	0.028	0.0027±0.0003	-40.6±15	-	-	-
24.07	440	pc-TMS-6P-TMS	MoO_3-Ag	SiO_2/PMMA	-	-	-	-	-	-
24.07	441	pc-TMS-6P-TMS	MoO_3-Ag	SiO_2/HMDS	0.006	0.0013±0.0001	-29.8±20	-	-	-
25.07	442	pc-MAF	MoO_3-Ag	SiO_2/HMDS	-	-	-	0.628	0.1350±0.0120	39.9±14
25.07	443	pc-MAF	MoO_3-Ag	SiO_2/HMDS	-	-	-	0.558	0.0979±0.0100	45.90±11

Table 2: Oligophenylenes (4p, 5p and 6p) attempt 2.

Finally, it has to be noted that both dielectric layers (HMDS and PMMA) show significant deviations from ideal characteristics (hysteresis, large threshold voltage), which affects the reliability of the extracted mobility values. As the difference between the average mobilities found on HMDS vs. PMMA are only a factor four, it cannot be stated with certainty that HMDS is the superior dielectric layer for this compound.

OLET Luminescence Program

The goal of this task was to design a program that could extract the light intensity and position as a function of gate voltage V_g and the result is shown in figure 12. The data in the figures was extracted from a video of light emission during a transfer measurement of device 393 based on a TMS-T4PT-TMS active layer.

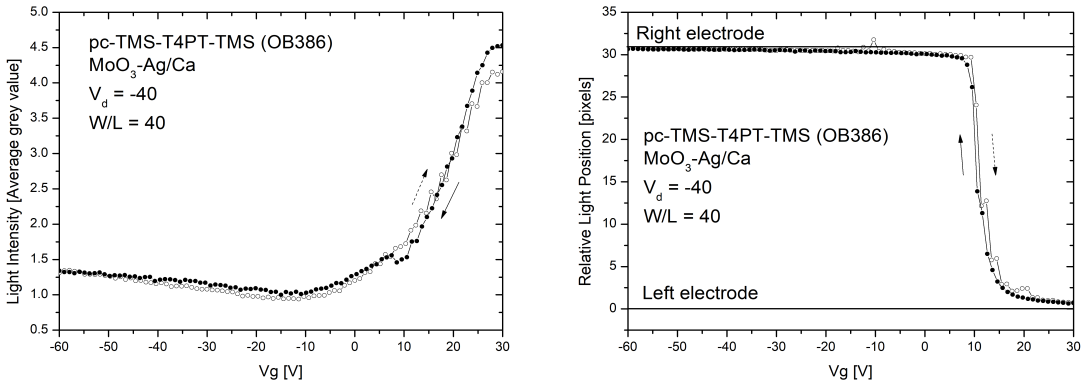

Figure 12: OLET Light intensity (left) and position (right) as a function of gate bias V_g.

The figures show that the light intensity is the highest at the left electrode and that the light moves from the left to the right electrode upon decrease of the gate potential. The light is for only a small gate voltage range (8 - 15 V) located within the channel. For all other gate voltages, light emission occurs at the electrode-semiconductor interface. Finally, the figures suggest that the correct gate voltage was assigned to each frame, as the data points measured in forward and in backward direction overlap to a large extend.

4 Discussion/Conclusions

In summary, my individual work was focussed on $CsCO_3$ electrodes, Oligophenylene active layers, and a program for OLET luminescence analysis. No evidence for superior electron injection capabilities of $CsCO_3$-Al electrodes was found. In contrast, evidence for lower contact resistance using Ca electrodes was observed in the output characteristics. The poor performance of the $CsCO_3$-Al electrodes is believed to be the result of complications during the evaporation of the Al layer resulting in oxidation of the electrode. (layer was formed in three separate stages during exp 412 & 413 and formed at a low rate of 0.4 Å/s during exp 418 and 419). These problems motivated to try a new evaporation method in which Al was evaporated from crucible, but time did not allow to repeat these experiments.

The experiments on the oligophenylenes (4P, 5P and TMS-6P-TMS), showed a decrease in device performance upon increasing the oligomer length. Whereas a maximum hole mobility of 0.0408 $cm^2V^{-1}s^{-1}$ was observed for 4P on HMDS, significantly smaller maximum mobilities of 0.0276 $cm^2V^{-1}s^{-1}$ and 0.0057 $cm^2V^{-1}s^{-1}$ were observed for 5P and TMS-6P-TMS respectively. A similar tendency was found for the statistically more significant average hole mobilities which were found to approximately halve for each extra phenylene group. It has to be noted that significant hysteresis was observed during gate voltage sweeps. This in combination with large threshold voltages and degradation in output curves are features of non-ideal OFET characteristics which affects the applicability of the Shockley equations (eq. 4 and 5) for accurate mobility extraction. Therefore, efforts are needed to identify and eliminate the origin of these features such that more significant statistics on the effect of Oligomer length on device performance can be obtained.

The OLET Luminescence analysis program was successfully made and tested on multiple videos of OLET light emission during transfer measurements. The program was found to accurately extract the relative light intensity (mean greyscale) and light position (relative to the left electrode) as a function of the gate voltage. For future use and program maintenance all functions were commented and given logical names corresponding to their task. A description of the programs functionality and users information are given in the appendix.

Bibliography

[1] A. F. Paterson, S. Singh, K. J. Fallon, T. Hodsden, Y. Han, B. C. Schroeder, H. Bronstein, M. Heeney, I. McCulloch, and T. D. Anthopoulos, "Recent Progress in High-Mobility Organic Transistors: A Reality Check," *Advanced Materials*, vol. 30, no. 36, pp. 1–33, 2018.

[2] R. H. Friend, A. R. Brown, D. D. C. Bradley, J. H. Burroughes, N. C. Greenham, P. L. Burn, A. B. Holmes, and A. M. Kraft, "Light-emitting diodes based on conjugated polymers," *Nature*, vol. 347, no. 6293, p. 539, 1990.

[3] Sirringhaus, Henning, Tessler, Nir, and Friend, Richard H., "Integrated Optoelectronic Devices Based on Conjugated Polymers," *Science*, vol. 280, no. 5370, pp. 1741–1744, 1998.

[4] C. Rost, S. Karg, W. Ries, M. A. Loi, M. Murgia, and M. Muccini, "Ambipolar light-emitting organic field-effect transistor," *Applied Physics Letters*, vol. 85, no. 9, pp. 1613–1615, 2004.

[5] J. Liu, H. Zhang, H. Dong, L. Meng, L. Jiang, L. Jiang, Y. Wang, J. Yu, Y. Sun, W. Hu, and A. J. Heeger, "High mobility emissive organic semiconductor," *Nature Communications*, vol. 6, no. May, 2015.

[6] S. Z. Bisri, T. Takenobu, and Y. Iwasa, "The pursuit of electrically-driven organic semiconductor lasers," *Journal of Materials Chemistry C*, vol. 2, no. 16, pp. 2827–2836, 2014.

[7] H. H. Choi, K. Cho, C. D. Frisbie, H. Sirringhaus, and V. Podzorov, "Critical assessment of charge mobility extraction in FETs," *Nature Materials*, vol. 17, no. 1, pp. 2–7, 2017.

[8] O. D. Parashchuk, A. A. Mannanov, V. G. Konstantinov, D. I. Dominskiy, N. M. Surin, O. V. Borshchev, S. A. Ponomarenko, M. S. Pshenichnikov, and D. Y. Paraschuk, "Molecular Self-Doping Controls Luminescence of Pure Organic Single Crystals," *Advanced Functional Materials*, vol. 28, no. 21, pp. 1–9, 2018.

[9] A. R. Brown, C. P. Jarret, D. M. De Leeuw, and M. Matters, "Field-effect transistors made from solution-processed organic semiconductors," *Synthetic Metals*, vol. 88, no. 1, pp. 37–55, 1997.

[10] Z. Bao and J. Locklin, *Organic Field-Effect Transistors*. 2007.

[11] Y. Xu, H. Sun, and Y. Y. Noh, "Schottky Barrier in Organic Transistors," *IEEE Transactions on Electron Devices*, vol. 64, no. 5, pp. 1932–1943, 2017.

[12] E. C. Smits, T. D. Anthopoulos, S. Setayesh, E. Van Veenendaal, R. Coehoorn, P. W. Blom, B. De Boer, and D. M. De Leeuw, "Ambipolar charge transport in organic field-effect transistors," *Physical Review B - Condensed Matter and Materials Physics*, vol. 73, no. 20, pp. 1–9, 2006.

[13] E. C. Smits, S. G. Mathijssen, M. Cölle, A. J. Mank, P. A. Bobbert, P. W. Blom, B. De Boer, and D. M. De Leeuw, "Unified description of potential profiles and electrical transport in unipolar and ambipolar organic field-effect transistors," *Physical Review B - Condensed Matter and Materials Physics*, vol. 76, no. 12, pp. 1–6, 2007.

[14] M. Bronner, A. Opitz, and W. Brütting, "Ambipolar charge carrier transport in organic semiconductor blends of phthalocyanine and fullerene," *Physica Status Solidi (A) Applications and Materials Science*, vol. 205, no. 3, pp. 549–563, 2008.

[15] L. G. Kudryashova, M. S. Kazantsev, V. A. Postnikov, V. V. Bruevich, Y. N. Luponosov, N. M. Surin, O. V. Borshchev, S. A. Ponomarenko, M. S. Pshenichnikov, and D. Y. Paraschuk, "Highly Luminescent Solution-Grown Thiophene-Phenylene Co-Oligomer Single Crystals," *ACS Applied Materials and Interfaces*, vol. 8, no. 16, pp. 10088–10092, 2016.

[16] T. S. Huang, Y. K. Su, and P. C. Wang, "Poly(methyl methacrylate) dielectric material applied in organic thin film transistors," *Japanese Journal of Applied Physics*, vol. 47, no. 4 PART 2, pp. 3185–3188, 2008.

[17] S. C. Lim, S. H. Kim, J. H. Lee, M. K. Kim, D. J. Kim, and T. Zyung, "Surface-treatment effects on organic thin-film transistors," *Synthetic Metals*, vol. 148, no. 1, pp. 75–79, 2005.

[18] K. K. Wasa and I. K. Hidetoshi, *Handbook of sputter deposition technology: fundamentals and applications for functional thin films, nano-materials and MEMS*. William Andrew, 2012.

[19] J. Huang, Z. Xu, and Y. Yang, "Low-work-function surface formed by solution-processed and thermally deposited nanoscale layers of cesium carbonate," *Advanced Functional Materials*, vol. 17, no. 12, pp. 1966–1973, 2007.

[20] G. Zuo, M. Linares, T. Upreti, and M. Kemerink, "General rule for the energy of water-induced traps in organic semiconductors," *Nature Materials*, vol. 18, no. 6, pp. 588–593, 2019.

Appendix

Individual Work

Date	Exp.	Act. Layer	Electrodes	Substrate	$\mu_{h,max}$	$\mu_{h,av.}$	V_e	$\mu_{e,max}$	$\mu_{e,av.}$	V_e
30.05	381	MAF	Ca	SiO_2/PMMA	-	-	-	0.039	0.0168±0.0005	20±5
30.05	382	MAF	Ca	SiO_2/HMDS	-	-	-	0.065	0.0338±0.0011	24±7

Table 3: PMMA vs. HMDS (Skill test evaporation)

Date	Exp.	Act. Layer	Electrodes	Substrate	$\mu_{h,max}$	$\mu_{h,av.}$	V_h	$\mu_{e,max}$	$\mu_{e,av.}$	V_e
24.06	406	pc-4P	MoO_3-Ag/Ca	SiO_2/PMMA	0.014	0.0039±0.0003	-25±12	-	-	-
24.06	407	pc-4P	MoO_3-Ag/Ca	SiO_2/HMDS	0.011	0.0034±0.0005	-53±18	-	-	-
24.06	408	MAF	MoO_3-Ag/Ca	SiO_2/HMDS	-	-	-	0.018	0.0064±0.0006	27±9
02.07	409	pc-5P	MoO_3-Ag/Ca	SiO_2/PMMA	0.0058	0.0015±0.0002	-42±26	-	-	-
02.07	410	pc-5P	MoO_3-Ag/Ca	SiO_2/HMDS	0.0135	0.0030±0.0004	-32±36	-	-	-
02.07	411	MAF	MoO_3-Ag/Ca	SiO_2/HMDS	-	-	-	0.384	0.1120±0.0074	38±14
11.07	423	pc-6P	MoO_3-Ag/Ca	SiO_2/PMMA	-	-	-	-	-	-
11.07	424	pc-6P	MoO_3-Ag/Ca	SiO_2/HMDS	0.00675	0.0008±0.0002	-36±30	-	-	-
11.07	425	MAF	MoO_3-Ag/Ca	SiO_2/HMDS	-	-	-	0.108	0.0453±0.0037	30±12

Table 4: Oligophenylenes (4p, 5p and 6p) attempt 1

Work performed together with or under supervision of Vasya Trukhanov

Date	Exp.	Act. Layer	Electrodes	Substrate	$\mu_{h,max}$	$\mu_{h,av.}$	V_h	$\mu_{e,max}$	$\mu_{e,av.}$	V_e
22.05	370	$P_fTP_fTP_f$	MoO_3-Ag/Ca	SiO_2/PMMA	-	-	-	0.002	0.0004±0.00004	37±19
22.05	371	$P_fTP_fTP_f$	MoO_3-Ag	SiO_2/PMMA	-	-	-	0.001	0.0004±0.00004	40±17
22.05	372	MAF	MoO_3-Ag	SiO_2/PMMA	-	-	-	0.272	0.0713±0.0029	37±7
22.05	373	MAF	MoO_3-Ag/Ca	SiO_2/PMMA	-	-	-	0.045	0.0237±0.0010	28±10
24.05	374	4FPhNDI[1]	Ca	SiO_2/HMDS	-	-	-	0.000	0.0000±0.0000	50±190
24.05	375	4FPhNDI[2]	Ca	SiO_2/HMDS	-	-	-	0.005	0.0028±0.0001	24±7
24.05	376	MAF	Ca	SiO_2/PMMA	-	-	-	0.033	0.0094±0.0005	29±6
05.06	387	DC-DBO	Ca	SiO_2/PMMA	-	-	-	-	-	-
05.06	388	DC-DBO	Ca	SiO_2/PMMA	-	-	-	0.002	0.0006±0.0001	60±72
05.06	389	DC-DBO	Ca	SiO_2/PMMA	-	-	-	0.053	0.0252±0.0020	25±26
14.06	397	DC-DBO	Ca	SiO_2/PMMA	-	-	-	-	-	-
14.06	399	PDI3	Ca	SiO_2/PMMA	-	-	-	0.001	0.0003±0.0004	-12±20

Table 5: n-channel OLETs

Date	Exp.	Act. Layer	Electrodes	Substrate	$\mu_{h,max}$	$\mu_{h,av.}$	V_h	$\mu_{e,max}$	$\mu_{e,av.}$	V_e
28.05	377	TMS-P4TP-TMS	MoO_3-Ag/Ca	SiO_2/HMDS	0.0431	0.022±0.003	-11±6	0.006	0.0017±0.0008	48±11
28.05	378	TMS-P4TP-TMS	MoO_3-Ag/Ca	SiO_2/PMMA	0.0047	0.002±0.0004	-14±6	0.001	0.0004±0.0001	33±9
28.05	379	MAF	MoO_3-Ag/Ca	SiO_2/HMDS	-	-	-	0.647	0.0793±0.0090	24±12
28.05	380	MAF	MoO_3-Ag/Ca	SiO_2/PMMA	-	-	-	0.121	0.0265±0.0020	16±9
06.06	390	OB386	MoO_3-Ag/Ca	SiO_2/PMMA	0.0118	0.00281±0.00018	-10.6±8	0.010	0.0014±0.0003	30.8±7
06.06	391	MAF	MoO_3-Ag/Ca	SiO_2/PMMA	-	-	-	0.013	0.0050±0.0003	31±12
14.06	398	TMS-P4TP-TMS	MoO_3-Ag/Ca	SiO_2/PMMA	0.018	0.0076±0.001	-8±5	0.001	0.0006±0.0001	44±7
14.06	400	MAF	MoO_3-Ag/Ca	SiO_2/PMMA	-	-	-	0.006	0.0046±0.0002	37±5

Table 6: P4TP (ambipolar)

Luminescence Program

Program Functionality Description

1. The light of all frames in the video is integrated into a single image resulting in an image similar to figure 13a.

2. Based on this image, the user is asked to select a rectangular region of interest (ROI). All remaining pixels beyond the ROI are ignored for the purpose of noise reduction.

3. Using the integrated image, the software determines the position of the left electrode based on a sharp increase in pixel brightness.

   (a) The coordinates of the brightness step is determined at n equidistant vertical positions, where n is the number of 'fitlines' selected by the user.

   (b) The electrode position is approximated by a linear fit through these coordinates

   (c) In order to account for curvature, the image can be divided into s, user defined, different sections, each in which the previous two steps are performed.

4. Subsequently each frame is analysed separately and the light intensity and coordinates are determined

   (a) Relative light intensity is determined by averaging the greyscale of all pixels.

   (b) After the greyscale is determined, a median filter, "*medfilt2*", is applied to eliminate noise and to highlight the light. By taking the median in a rectangular box, stretched in the vertical direction (30 by 2 pixels was found to be optimal), vertically bright features (i.e. OLET light emission) are highlighted and noise is removed.

   (c) The horizontal light coordinates are determined at n vertical positions in s sections based on the weighted average horizontal position with pixel intensities used as weight factors.

   (d) Within each section, the light position is approximated by a linear fit through the n obtained coordinates.

5. The relative light position is determined

   (a) In each section n equidistant lines, perpendicular to the electrode are defined.

   (b) The relative light position then follows from averaging the distance it takes each perpendicular line to intersect with the line representing the light.

6. The gate voltage, V_g, corresponding to each frame is determined.

   (a) Gate voltage is determined based on hysteresis of the transfer measurements resulting in a symmetrical light intensity vs. frame plot. Using the MATLAB function *findpeaks*, two frames with identical V_g are identified.

   (b) Next from the video framerate and the transfer measurement parameters ($V_{g,start}$, $V_{g,stop}$, # points, delay between points), each frame can be assigned an accurate approximation of V_g.

7. ASCII data on Relative light intensity and position is saved for each section separately.

Use of the Program

A simple graphical user interface (GUI) was made for easy use of the program. It enables the user the select the video file and the preferential number of sections and fit points. Furthermore it offers several options concerning the data that has to be saved. Individual frames and a cropped video of the ROI can be saved allowing the user to judge the programs capability of finding the correct positions for light and electrode.

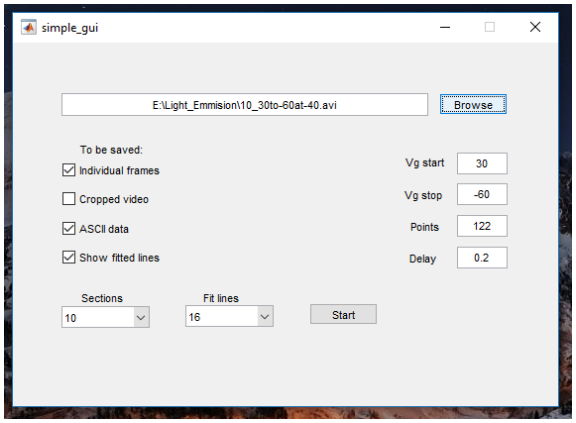

Figure 13: Shadow effect resulting in asymmetrical source-drain geometry for efficient hole and electron injection.

Finally, before starting the program, the user has to provide the biasing conditions used for the transfer measurement corresponding to the selected video. Based on these values, the program is able to determine the gate voltage V_g corresponding to each frame. The user interface appears upon selecting the function *startGui.m* in the folder *Light-Emission.m*.

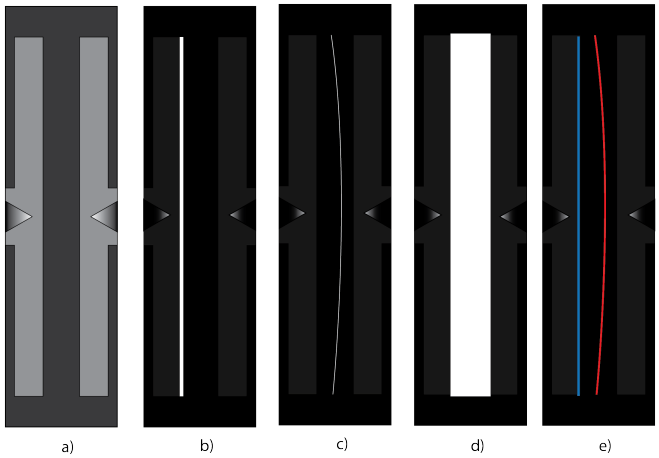

Figure 14: a) schematic top-view of device with light turned on. Light grey bars depict electrodes whereas triangles represent probes. b) Light emission starting at electrode-channel interface. c) Light emission moving from left to right electrode by changing the gate potential V_g. Light position is found in this frame by taking a weighted average of the horizontal pixel position, based on pixel brightness. d) Sum frame in which light of all frames in video is integrated. The sum frame is used for two purposes: Selection of ROI and determination of electrode-channel interface. e) Same frame as depicted in c), showing the programs approximation of electrode and light position, shown in blue and red respectively. The relative light position for the current frame, is calculated as the average distance between the two lines.

5P and 6P electrical characterization

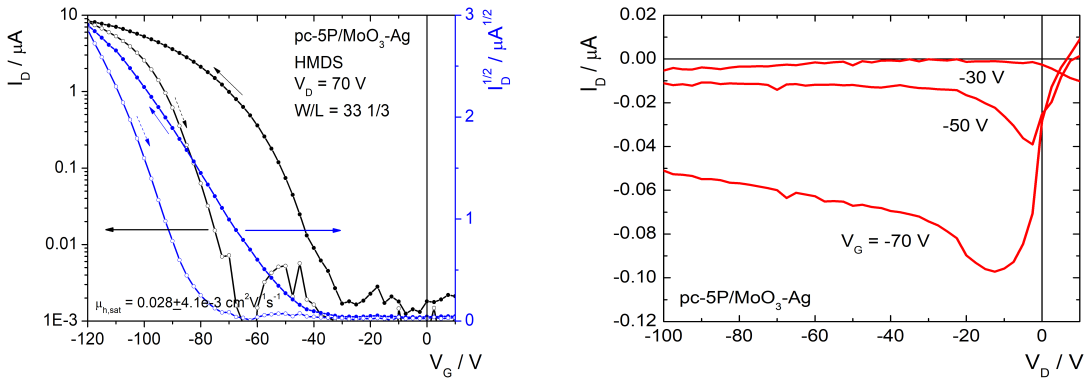

Figure 15: Electrical characterization of 6P Oligophenylene with Left: transfer- and right: output characteristics. Small source-gate leakages were observed in the transfer plot when $V_g \geq -60$ which explains the sudden rise of I_d at this point in the transfer plot.

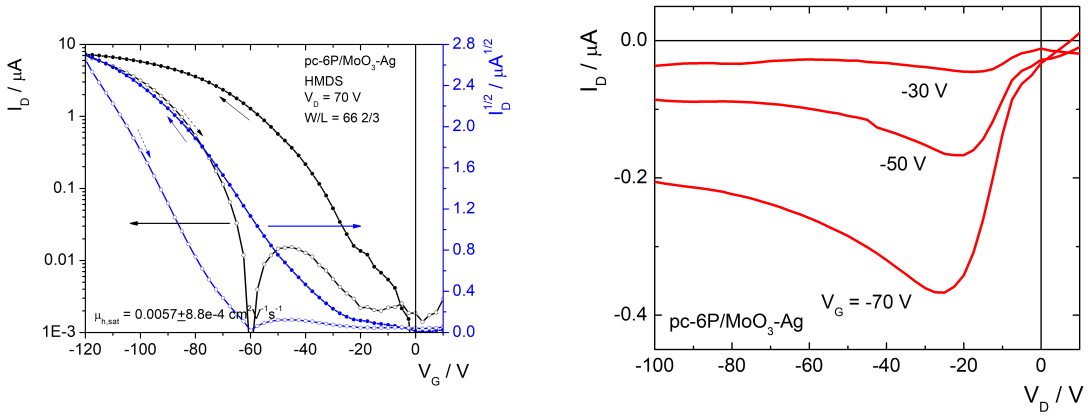

Figure 16: Electrical characterization of 6P Oligophenylene with Left: transfer- and right: output characteristics. Small source-gate leakages were observed in the transfer plot when $V_g \geq -60$ which explains the sudden rise of I_d at this point in the transfer plot.